Buffer-Layer-Assisted Epitaxial Growth of Perfectly Aligned Oxide Nanorod Arrays in Solution

ARTICLE *in* CRYSTAL GROWTH & DESIGN · OCTOBER 2011

Impact Factor: 4.89 · DOI: 10.1021/cg2007149

CRYSTAL GROWTH & DESIGN

ARTICLE

pubs.acs.org/crystal

Buffer-Layer-Assisted Epitaxial Growth of Perfectly Aligned Oxide Nanorod Arrays in Solution

Gong Ping Li,[†] Lin Jiang,[‡] Shi Jie Wang,[§] Xiao Wei Sun,[∥] Xiaodong Chen,[‡] and Tom Wu*[,†]

[†]Division of Physics and Applied Physics, School of Physical and Mathematical Sciences, Nanyang Technological University, Singapore 637371, Singapore

[‡]School of Materials Science and Engineering and [∥]School of Electrical & Electronic Engineering, Nanyang Technological University, Singapore 639798, Singapore

[§]Materials Science and Characterization Cluster, Institute of Materials Research and Engineering, Singapore 117602, Singapore

Supporting Information

ABSTRACT:

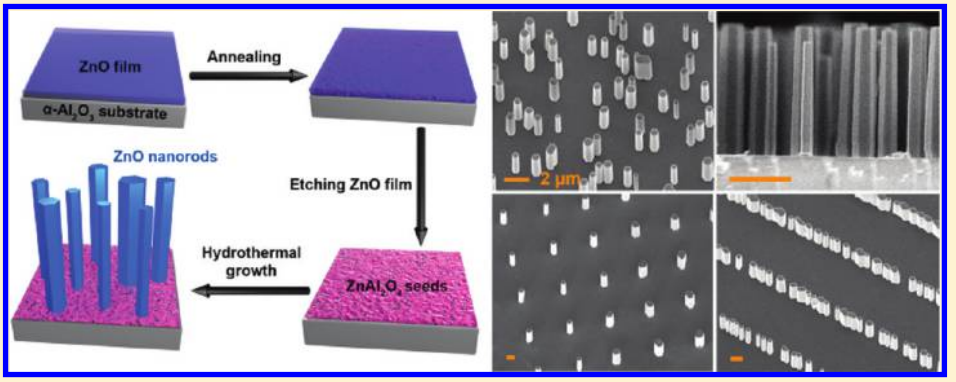

Epitaxy between materials with good lattice match requires perfect staking on the atomic scale and is thus often considered to be challenging to achieve by low-temperature solution-based hydrothermal growth. Inspired by the concept of the buffer layer in vapor-phase epitaxial growth, we present herein a novel synthetic protocol of employing $ZnAl_2O_4$ epilayers to hydrothermally grow perfectly aligned ZnO nanorod arrays in solution. Remarkable tunability of the density and dimensions of the nanorods can be realized by adjusting the roughness of the $ZnAl_2O_4$ layer and the nutrient solution concentration, which is in line with the classical nucleation theory and also confirms that the nanorod growth is mass-transport-limited. Furthermore, through nanopatterning of the $ZnAl_2O_4$ layer by electron beam lithography, shape-controlled vertical ZnO nanostructures at predesigned positions can be achieved. Finally, taking advantage of the epitaxial relationships, we adjusted the tilting orientations of the aligned nanorods by selecting sapphire substrates with different surface planes.

INTRODUCTION

The integration of semiconductor nanostructures into functional nanodevices requires the development of new strategies with effective control on orientation, dimension, density, and position. Low-temperature solution-based synthesis is facile and economical and has thus attracted much attention in recent years.[1−6] In particular, hydrothermal growth is considered to be well suited to growing ZnO nanostructures, for example, nanorods (NRs) or nanowires (NWs), that have been intensively pursued for applications such as light emission,[7−9] solar cells,[10] field-emission devices,[11−13] wettability-controlled coatings,[14] nanogenerators,[15,16] and nanolasers.[17−20]

However, it is often considered that the drawback of hydrothermal solution synthesis is a lack of control, which is a trade-off with the fact that the method is fast and economical. Although there have been significant developments on seeding and patterning methods toward the rational hydrothermal synthesis of ZnO NRs,[21−28] some difficulties still remain to be confronted. One is finding effective seeding strategies to produce vertically aligned NRs. Whereas textured ZnO nanocrystalline seeds are widely used to improve the out-of-plane orientation of ZnO NRs (shown in Figure 1a,b),[10,22,23] perfectly aligned ZnO NRs can grow only from unseeded substrates with very good lattice match.[29−33] In addition, if a ZnO seeding layer becomes part of the final product underneath the ZnO NRs, it can interfere with the functionalities of NR-array-based devices. Another challenge is to tune the density of vertically aligned NRs over a reasonably wide range, which is vital for obtaining optimal performances, such as field-emission and photovoltaic properties, in NR-array based devices.[12,34] In this work, the question we aimed to address is:

Received: June 8, 2011
Revised: August 23, 2011
Published: September 13, 2011

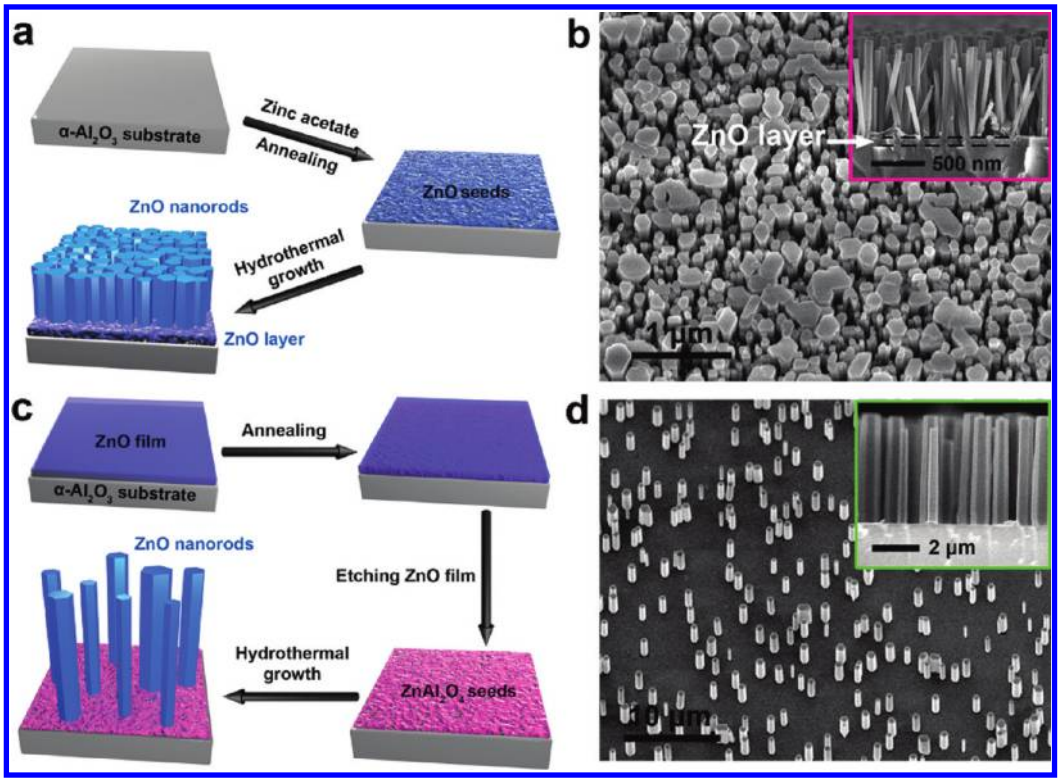

Figure 1. Schematics comparing the growth behaviors of ZnO NRs on the (a) commonly used ZnO seeded α-sapphire substrates and (c) $ZnAl_2O_4$ buffered α-sapphire substrates proposed in this work. (b,d) Corresponding SEM images of the growth products. A $Zn(NO_3)_2$ concentration of 20 mM was used in the hydrothermal growth. The cross-sectional SEM image in the inset of b highlights the ZnO seeding layer underneath the ZnO NRs, and the inset of d shows that the perfect alignment of ZnO NRs emerged only when the $ZnAl_2O_4$ buffer layer was used.

Can perfectly aligned ZnO NRs be synthesized in solution on commonly used sapphire substrates with good control of density and morphology?

The critical issue is rooted in the nucleation stage of growth: Analogous symmetry and small lattice mismatch often lead to high densities of ZnO crystal nuclei and uncontrolled growth.[30,35] When searching for approaches to achieve effectively controlled growth of ZnO nanomaterials, a buffer-layer-based approach with $ZnAl_2O_4$ particularly attracted our attention. $ZnAl_2O_4$ has the same crystal structure (cubic spinel) as $MgAl_2O_4$ and a similar lattice parameter (8.0867 vs 8.0831 Å), and (111) $MgAl_2O_4$ has been used to grow aligned ZnO NRs.[33] Therefore, our hypothesis is that $ZnAl_2O_4$ might present a similar epitaxial relationship with ZnO and initiate hydrothermal growth of high-quality ZnO nanomaterials. Furthermore, $ZnAl_2O_4$ has a wider band gap (~3.8 eV) than ZnO, so that it is inactive in the luminescence region of ZnO. Most importantly, $ZnAl_2O_4$ can readily form at the interface between ZnO and Al_2O_3 through a solid-phase reaction,[36] which potentially simplifies the synthesis procedure.

In the current work, we realized the growth of perfectly aligned ZnO NRs on $ZnAl_2O_4$-epilayer-coated sapphire substrates through a hydrothermal method. The matched lattice parameters between ZnO and $ZnAl_2O_4$ guarantee the epitaxial growth of ZnO NRs. By carefully designing the $ZnAl_2O_4$ epilayer, we achieved superior controls over the density, dimensions, position, orientation, and morphology of the ZnO NRs. Overall, the $ZnAl_2O_4$ epilayer presents much more effective controllability of the growth of ZnO NRs than the existing hydrothermal strategies.

EXPERIMENTAL SECTION

Materials. *Preparation of Substrates.* (i) For density-controlled growth of ZnO NRs, a ZnO thin film was prepared by the sol−gel method. Mixtures of zinc acetate dihydrate, 2-methoxyethanol, and monoethanolamine were used. The molar ratio of monoethanolamine to zinc acetate was maintained at 1.0. Details of this process were described elsewhere.[37] After being deposited on an α-sapphire substrate by spin coating, the film was baked on a hot plate at 300 °C for 10 min and then inserted into a furnace to anneal in air at temperatures from 800 to 1000 °C for 1 h to form the $ZnAl_2O_4$ layer. Subsequently, the residual ZnO was etched in diluted HCl acid and washed with deionized water. (ii) For position-controlled growth of ZnO nanostructures, the patterns were defined using electron beam lithography (EBL) on a JEOL JSM-6360 scanning electron microscope with a Raith Elphy quantum lithography attachment system. A 110-nm layer of 50k poly(methyl methacrylate) (PMMA) was spun on the α-sapphire substrate and then baked on a hot plate at 180 °C for 2 min. One-dimensional groove and hole patterns were generated using doses ranging from 10 to 50 $\mu C/cm^2$. After electron beam exposure, a 30-nm zinc film was sputtered on the substrate and then lifted off. Then, the patterned zinc film was annealed in air at 900 °C for 1 h and etched in diluted acid to remove the residual ZnO.

Hydrothermal Growth of ZnO Nanostructures. The reaction nutrient solution was composed of zinc nitrate hexahydrate $[Zn(NO_3)_2 \cdot 6H_2O]$ and hexamethylenetetramine (HMTA) (1:1 ratio). The zinc nitrate concentration was adjusted from

dx.doi.org/10.1021/cg2007149 |*Cryst. Growth Des.* 2011, 11, 4885–4891

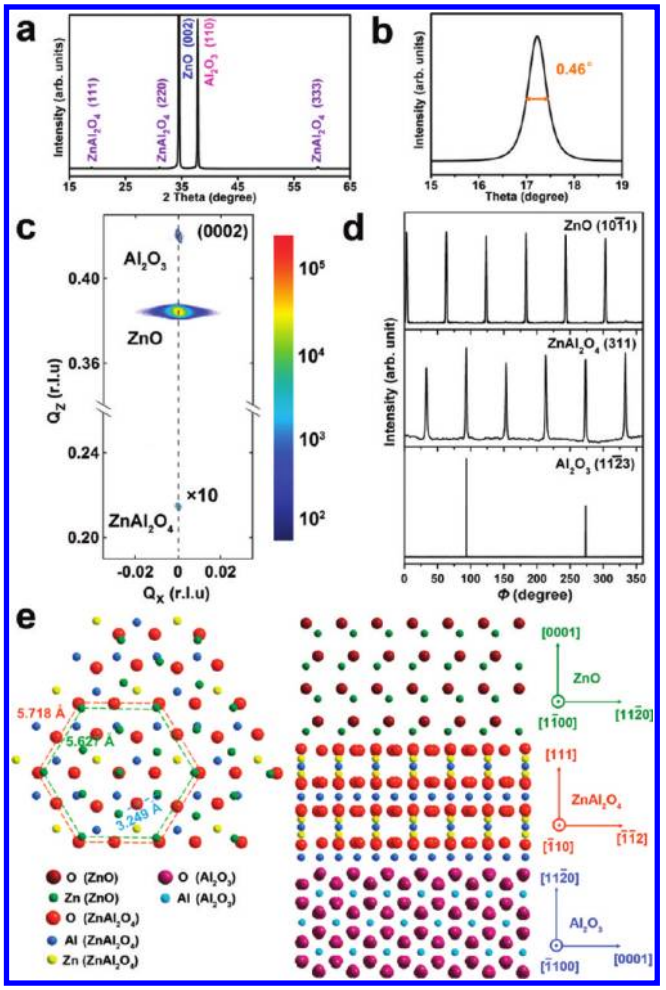

Figure 2. (a) XRD $\theta-2\theta$ pattern of the ZnO NRs grown on the $ZnAl_2O_4$-buffered α-sapphire substrate. (b) Corresponding rocking curve of the ZnO (0002) peak. (c) HL-mesh contour reciprocal space mapping (RSM) around the (0002) diffraction of ZnO. (The reciprocal lattice unit is abbreviated as rlu; Q_x and Q_z correspond to H and L, respectively.) (d) Off-axis ϕ scans along the azimuthal circle of the ZnO $\{10\bar{1}1\}$, $ZnAl_2O_4$ {311}, and Al_2O_3 $\{11\bar{2}3\}$ diffractions. (e) Atomic configuration of the epitaxy among (0001) ZnO, (111) $ZnAl_2O_4$, and $(11\bar{2}0)$ Al_2O_3. The lattice mismatch between (0001) ZnO and (111) $ZnAl_2O_4$ is ~1.6%.

5 to 100 mM to study its effect on the growth of ZnO NRs. The prepared substrates were immersed face down into the solution and heated to 70 °C for 12 h. After being allowed to cool to room temperature, the substrates were washed with deionized water and dried in air at 70 °C for 30 min.

Characterization. The crystal structure and morphology of the samples were studied by X-ray diffraction (XRD) (Rigaku SmartLab X-ray diffractometer and Bruker D8 Advanced X-ray diffractometer) and scanning electron microscopy (SEM) (JEOL JSM-6700F). The topographies of the $ZnAl_2O_4$-coated sapphire substrates were probed by atomic force microscopy (AFM) (Veeco Digital Instruments). The chemical composition was determined by X-ray photoelectron spectroscopy (XPS) (VG ESCALAB 220i-XL system equipped with a monochromatic X-ray source) in an ultra-high-vacuum chamber at a pressure lower than 1.0×10^{-9} Torr. Peak positions are referenced to the adventitious C 1s peak, which was taken to be 285.0 eV.

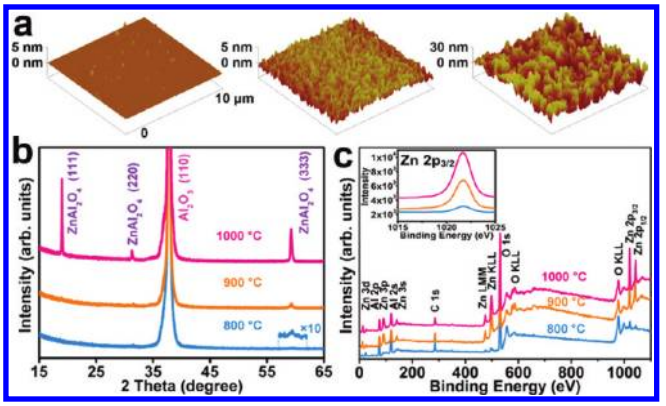

Figure 3. (a) AFM micrographs of $ZnAl_2O_4/\alpha$-sapphire substrates prepared by annealing at 800, 900, and 1000 °C. Their rms roughnesses are 0.413, 0.792, and 7.146 nm, respectively. It can be seen that, at lower annealing temperatures, the sapphire surface is modified at only some localized small patches, whereas higher annealing temperatures cause more significant changes of the surfaces. The corresponding (b) XRD and (c) XPS spectra of these samples also confirm the annealing effect. The inset in c presents the enlarged Zn $2p_{3/2}$ peaks in the XPS spectra.

RESULTS AND DISCUSSION

Density-Controlled Growth of Vertical ZnO NRs. According to a previous report[38] and our own experiments, smooth surfaces of the bare sapphire substrates cannot provide effective nucleation sites for the growth of ZnO nanostructures in aqueous solution. To create nucleation sites in a controllable way, a new flow of synthesis procedures was applied, as illustrated in Figure 1c. First, we spin-coated a ZnO layer on an α-sapphire substrate using the sol−gel method. After annealing in air and subsequent etching in diluted acid to remove the residual ZnO, a thin $ZnAl_2O_4$ layer was formed on the substrate. Then, ZnO NRs were grown on this $ZnAl_2O_4$-coated sapphire substrate through the conventional hydrothermal route at a low temperature (70 °C). Removing the top residual ZnO layer is a critical step to expose the fresh $ZnAl_2O_4$ buffer layer; otherwise, the control of the subsequent hydrothermal growth would be compromised.

The SEM image in Figure 1d shows that the NRs had perfect vertical alignment, which corroborates the narrow full-width-at-half-maximum (fwhm) of the rocking curve of the ZnO (0002) plane (Figure 2b). The cross-sectional SEM image indicates that no ZnO buffer layer was present at the bottom of the NRs (inset of Figure 1d). The nanorods had a well-defined hexagonal shape with an average height of 3.9 μm and an average diameter of 0.8 μm. In the XRD pattern, several weak $ZnAl_2O_4$ peaks were detected, in addition to the ZnO and Al_2O_3 peaks (Figure 2a). The out-of-plane orientations were further investigated by reciprocal space mapping (RSM) around the (0002) diffraction of ZnO (Figure 2c). The diffraction peaks of ZnO (0002), $ZnAl_2O_4$ (111), and Al_2O_3 $(11\bar{2}0)$ were located at the same H value ($H = 0$), indicating the epitaxial relationship of $(0001)_{ZnO} \parallel (111)_{ZnAl_2O_4} \parallel (11\bar{2}0)_{Al_2O_3}$. The in-plane epitaxial relationships were further evaluated by measuring the off-axis ϕ scans of ZnO $\{10\bar{1}1\}$, $ZnAl_2O_4$ {311}, and Al_2O_3 $\{11\bar{2}3\}$ diffractions, as shown in Figure 2d. The 30° separation between the NRs and the $ZnAl_2O_4$ epilayer (as well as the sapphire substrate) reveals an in-plane orientation of ZnO $[11\bar{2}0] \parallel ZnAl_2O_4$ $[\bar{1}\bar{1}2] \parallel Al_2O_3$ [0001]. Figure 2e illustrates the atomic configuration of the epitaxial relationship of (0001) ZnO $\parallel$ (111) $ZnAl_2O_4 \parallel$ $(11\bar{2}0)$

dx.doi.org/10.1021/cg2007149 |Cryst. Growth Des. 2011, 11, 4885–4891

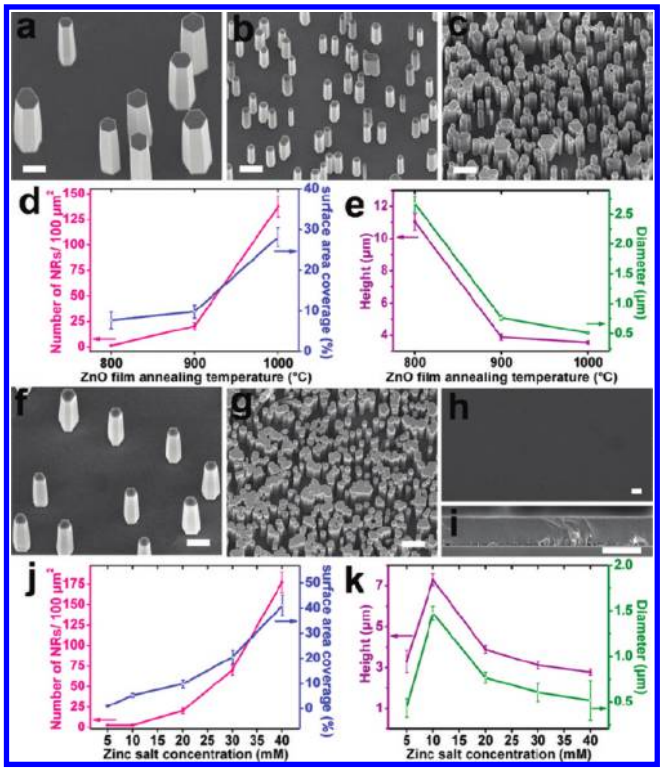

Figure 4. SEM images of ZnO NRs fabricated on $ZnAl_2O_4/\alpha$-sapphire substrates created by annealing at (a) 800, (b) 900, and (c) 1000 °C, with $[Zn(NO_3)_2]$ = 20 mM. (d,e) Dependences of density, surface area coverage, and dimensions (height and diameter) on the formation temperature of the $ZnAl_2O_4$ epilayer. SEM images of ZnO NRs grown on $ZnAl_2O_4/\alpha$-sapphire substrates prepared at 900 °C, with $[Zn(NO_3)_2]$ = (f) 10, (g) 40, and (h,i) 100 mM. (j,k) Dependences of density, surface area coverage, and dimensions (height and diameter) on $Zn(NO_3)_2$ concentration. All scale bars represent 2 μm.

Al_2O_3. The small lattice mismatch between (0001) ZnO and (111) $ZnAl_2O_4$ (~1.6%) is comparable with that in the (0001) ZnO/(111) $MgAl_2O_4$ case,[39] thus satisfying the essential conditions for ZnO epitaxy.

To probe the morphology evolution of this thin $ZnAl_2O_4$ layer, we annealed the ZnO film/α-sapphire substrates at three different temperatures for 1 h. After etching, the topographies of the residual ZnO were examined by AFM (Figure 3a). With increasing annealing temperature, the root-mean-square (rms) roughness of the substrates in an area of 10 × 10 μm^2 notably increased from 0.413 to 7.146 nm, which suggests a thermally accelerated reaction between ZnO and sapphire. This finding is consistent with the intensity enhancement of both the $ZnAl_2O_4$ peaks in the corresponding XRD spectra (Figure 3b) and the Zn $2p_{3/2}$ peaks in the XPS spectra (Figure 3c). We should note here that, whereas high-temperature annealing in air might not be compatible with in-line processing, alternatives such as laser annealing are available that would allow high-temperature treatments to be rapidly conducted in a localized manner with a controlled thermal budget.[40,41]

We further systematically studied the effect of synthesis parameters on the growth behaviors of the ZnO NRs. Remarkably, the density of the NRs increased with both the synthesis temperature of the $ZnAl_2O_4$ layer and the nutrient solution concentration, as shown in Figure 4 and Figure S1 (Supporting Information). When we changed the $ZnAl_2O_4$ synthesis temperature from 800 to 1000 °C while fixing the nutrient solution concentration at 20 mM, the average number of the ZnO NRs within an area of 100 μm^2 increased from 1.4 to 137.7. This corresponds to an increase of surface coverage from 7.7% to 28.1%. A density modulation with a similar magnitude can also be achieved by adjusting the nutrient solution concentration from 10 to 35 mM.

In classical nucleation theory,[42] the nucleation rate J can be written as

$$J \propto N \exp(-\Delta G/kT) \quad (1)$$

where N is the number of potential nucleation sites, ΔG is the activation barrier for nucleation, and k is the Boltzmann constant. A higher annealing temperature of the $ZnAl_2O_4$ layer increases its surface roughness (Figure 3a), resulting in more active nucleation sites. On the other hand, ΔG decreases with rising supersaturation, which can be induced by increasing the nutrient solution concentration. Therefore, both factors, namely, the synthesis temperature of the $ZnAl_2O_4$ epilayer and the nutrient solution concentration, can vary the nucleation rate, leading to a modulation of the NR density. In particular, if the Zn salt concentration reaches 100 mM, excessive lateral epitaxial overgrowth of ZnO generates a thick continuous film with no visible cracks (Figure 4h,i). Its quality is comparable to that of ZnO films grown on (111) $MgAl_2O_4$ substrates.[43] Such ZnO films are promising substrates for the epitaxial growth of other materials such as GaN, and if necessary, they can be easily removed by postgrowth lift-off and transferred onto other supporting substrates.

Interestingly, the growth parameters delineated above induce opposite effects on the dimensions (height and diameter) of the ZnO NRs (Figure 4e,k). In other words, the NR dimensions are reciprocally proportional to their density. A size modulation of larger than 1 order of magnitude can be induced by tuning the experimental conditions. This phenomenon conforms with the mass-transport-limited model proposed by Boercker et al.,[44] as well as other previous experiments.[24,45,46] According to the simple one-dimensional model, the concentration of the precursor can be written as

$$C(t) = \frac{C_\infty}{(1 + \Phi)} \quad (2)$$

where C_∞ is the initial concentration and Φ is a dimensionless Thiele modulus

$$\Phi = \frac{N(k_z \pi R^2 + 2k_r \pi R h)\delta}{D} \quad (3)$$

In this equation, D is the diffusion coefficient of the precursor; δ is the thickness of the concentration boundary layer; and k_z and k_r are the surface reaction rates on the top (0001) and side $(10\bar{1}0)$ surfaces, respectively, of the ZnO NRs. All of these factors can be regarded as constants. On the other hand, the density of the NRs, N; the radius of the NRs, R; and the height, h, are functions of time and Φ. When mass-transport-limited growth dominates (i.e., $\Phi \gg 1$), the higher density of NRs results in the more rapid depletion of precursor near the surface, inducing a slower growth of NRs. As a result, we have

$$h \propto N^{-1/3} \quad (4)$$

$$R \propto N^{-1/3} \quad (5)$$

As shown in Figure S2 (Supporting Information), the fitting curves from eqs 4 and 5 match well with our experimental data, confirming

that the growth of ZnO NRs is mass-transport-limited. It should be mentioned here that the dimensions are also proportional to the reaction time; that is, smaller NRs with a low density can be obtained by shortening the reaction time.[22]

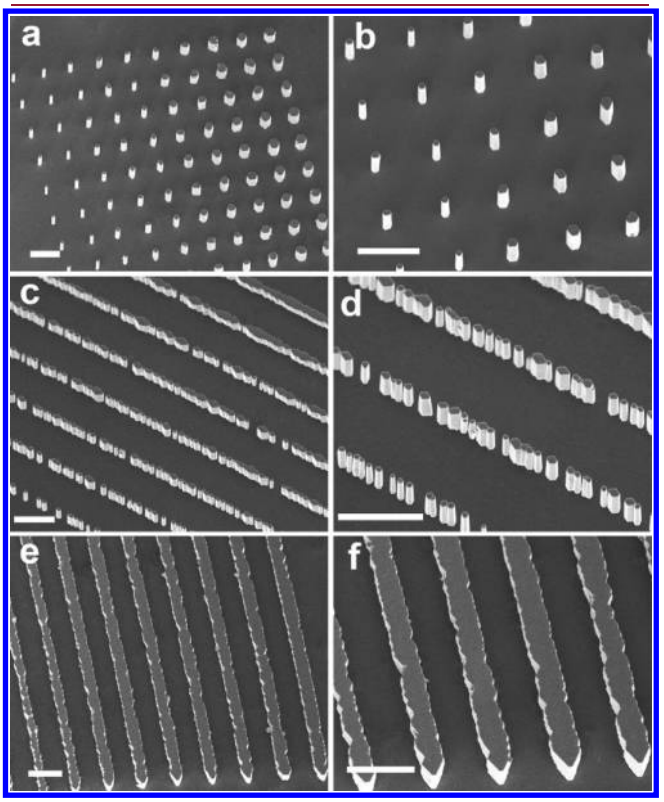

Figure 5. SEM images of ZnO (a,b) NR arrays, (c,d) NR rows, and (e,f) extended wall-like structures grown on EBL-patterned $ZnAl_2O_4$/α-sapphire substrates, with $[Zn(NO_3)_2]$ = 20 mM. The scale bars represent 10 μm.

Position- and Orientation-Controlled Growth of ZnO NRs. It is generally agreed that producing nanostructures at predesigned positions is crucial to nanodevice integration. As shown in Figure 5, by combining hydrothermal growth with the EBL technique, we successfully fabricated vertical ZnO nanostructures with predesigned patterns, ranging from NR arrays and rows to extended wall-like structures. First, by writing on the spin-coated PMMA resist with an electron beam, we defined holes with diameters from 0.5 to 2.5 μm and lines with widths from 0.3 to 3 μm while keeping the distance between the features at 10 μm. Then, a zinc layer of 30 nm was sputtered on the patterned PMMA. After lift-off, the fine zinc features were annealed in air at 900 °C, and the patterned $ZnAl_2O_4$ layer was finally obtained on the sapphire substrates after removal of the residual ZnO.

The positions of the NRs after the hydrothermal growth are strictly confined by the $ZnAl_2O_4$ template. This precise location control, however, is accompanied by a lateral size expansion: the diameters of the NRs in the arrays are ~3 times the sizes of the patterned $ZnAl_2O_4$ dots. For the growth of NR rows, interestingly, 500 nm is a critical width for the patterned $ZnAl_2O_4$ lines. In other words, when the $ZnAl_2O_4$ lines are thinner than 500 nm, NR rows are obtained; otherwise, the NRs coalesce to form extended wall-like structures. Moreover, with wider $ZnAl_2O_4$ lines, the width of the grown ZnO walls becomes more uniform with fewer grain boundaries. All of our experiments confirmed that the $ZnAl_2O_4$ epilayer can dramatically enhance the nucleation rate and promote the growth of ZnO NRs. We also prepared an α-sapphire substrate that was partially covered by $ZnAl_2O_4$, and subsequent hydrothermal growth showed that the ZnO NRs grew only on the $ZnAl_2O_4$-covered surface, whereas the smooth sapphire surface could not initiate any ZnO nucleation (Figure S3 in the Supporting Information).

In addition to the perpendicular orientation, it is desirable to have other kinds of ordering to cater to potential needs in nanodevice fabrication. In our case, this can be readily realized by employing sapphire substrates with different surface planes, which can tune the epitaxial orientation of the $ZnAl_2O_4$ seeding

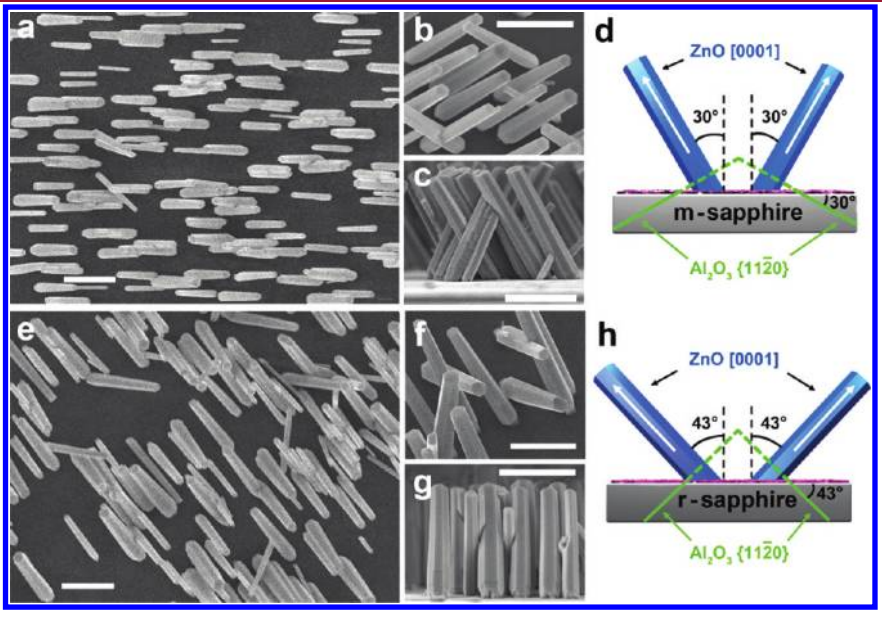

Figure 6. Top-view, 20°-tilted, and cross-sectional SEM images of ZnO NRs fabricated on (a−c) $ZnAl_2O_4$/*m*-sapphire substrate and (e−g) $ZnAl_2O_4$/*r*-sapphire substrate. $[Zn(NO_3)_2]$ = 20 mM. The $ZnAl_2O_4$ layers were formed by annealing ZnO/sapphire at 800 °C. All scale bars represent 2 μm. (d,h) Schematics illustrating the orientations of the ZnO NRs grown on the sapphire substrates with different surface terminations.

dx.doi.org/10.1021/cg2007149 |*Cryst. Growth Des.* 2011, 11, 4885–4891

layer and eventually result in ZnO NRs with uniform tilting angles. Figure 6a−c displays the oriented ZnO NRs grown on a $ZnAl_2O_4/(10\bar{1}0)$ sapphire (*m*-plane) substrate. Because the angle between the *m* plane and the *α* plane of sapphire is 30°, epitaxial growth of ZnO NRs along the [0001] direction induces a particular tilting of 30° from the normal of the *m* plane, as illustrated in Figure 6d. The uniformly tilted ZnO NRs can be grown on $ZnAl_2O_4/(1\bar{1}02)$ sapphire (*r*-plane) substrates as well, which gives a tilting angle of 43° from the normal direction of the substrates (Figure 6e−h). The good tunability of the tilting angles of the ZnO NRs indicates that this approach is universal and effective for solution-based synthesis, comparable to the conventional vapor-based routes.

CONCLUSIONS

In summary, we have developed a new surface engineering strategy to achieve epitaxial growth of perfectly aligned ZnO NRs by the commonly used hydrothermal method. By tuning the $ZnAl_2O_4$ buffer layer roughness and the nutrient solution concentration, NR density and dimensions were controllably modulated. Furthermore, patterned vertical ZnO nanostructures, such as NR arrays, rows, and extended wall-like structures were obtained by patterning the $ZnAl_2O_4$ layer using lithographic techniques. Finally, controlled growth of ZnO NRs with other particular orientations was obtained by using sapphire substrates with different surface planes. These perfectly aligned ZnO nanostructures synthesized by such a facile approach are promising for applications in high-performance electronic and photonic nanodevices.

ASSOCIATED CONTENT

Supporting Information. Fitting diameters and heights of NRs as functions of their density, SEM images of ZnO NRs grown on *α*-sapphire substrates partially covered with a thick $ZnAl_2O_4$ layer, and growth behaviors of ZnO NRs on $ZnAl_2O_4/(0001)$ sapphire (*c* plane) substrates and $MgAl_2O_4$ epilayer/*α*-sapphire substrates. This material is available free of charge via the Internet at http://pubs.acs.org.

AUTHOR INFORMATION

Corresponding Author

*E-mail: tomwu@ntu.edu.sg. Tel.: +65-65141047. Fax: +65-67941325.

ACKNOWLEDGMENT

This work was supported by the Singapore National Research Foundation (RCA-08/018 and NRF-RF2009-04). X.C. also thanked the support from the Centre for Biomimetic Sensor Science at NTU in Singapore.

REFERENCES

(1) Holmes, J. D.; Johnston, K. P.; Doty, R. C.; Korgel, B. A. *Science* **2000**, *287*, 1471.
(2) Tian, Z. R. R.; Voigt, J. A.; Liu, J.; McKenzie, B.; McDermott, M. J.; Rodriguez, M. A.; Konishi, H.; Xu, H. F. *Nat. Mater.* **2003**, *2*, 821.
(3) Xia, Y. N.; Yang, P. D.; Sun, Y. G.; Wu, Y. Y.; Mayers, B.; Gates, B.; Yin, Y. D.; Kim, F.; Yan, Y. Q. *Adv. Mater.* **2003**, *15*, 353.
(4) Milliron, D. J.; Hughes, S. M.; Cui, Y.; Manna, L.; Li, J. B.; Wang, L. W.; Alivisatos, A. P. *Nature* **2004**, *430*, 190.
(5) Wang, X.; Zhuang, J.; Peng, Q.; Li, Y. D. *Nature* **2005**, *437*, 121.
(6) Morin, S. A.; Bierman, M. J.; Tong, J.; Jin, S. *Science* **2010**, *328*, 476.
(7) Cole, J. J.; Wang, X.; Knuesel, R. J.; Jacobs, H. O. *Nano Lett.* **2008**, *8*, 1477.
(8) Xu, S.; Xu, C.; Liu, Y.; Hu, Y. F.; Yang, R. S.; Yang, Q.; Ryou, J. H.; Kim, H. J.; Lochner, Z.; Choi, S.; Dupuis, R.; Wang, Z. L. *Adv. Mater.* **2010**, *22*, 4749.
(9) Liu, K. W.; Chen, R.; Xing, G. Z.; Wu, T.; Sun, H. D. *Appl. Phys. Lett.* **2010**, *96*, 023111.
(10) Law, M.; Greene, L. E.; Johnson, J. C.; Saykally, R.; Yang, P. D. *Nat. Mater.* **2005**, *4*, 455.
(11) Bai, X. D.; Wang, E. G.; Gao, P. X.; Wang, Z. L. *Nano Lett.* **2003**, *3*, 1147.
(12) Wang, X. D.; Zhou, J.; Lao, C. S.; Song, J. H.; Xu, N. S.; Wang, Z. L. *Adv. Mater.* **2007**, *19*, 1627.
(13) Xing, G. Z.; Fang, X. S.; Zhang, Z.; Wang, D. D.; Huang, X.; Guo, J.; Liao, L.; Zheng, Z.; Xu, H. R.; Yu, T.; Shen, Z. X.; Huan, C. H. A.; Sum, T. C.; Zhang, H.; Wu, T. *Nanotechnology* **2010**, *21*, 255701.
(14) Li, G. P.; Chen, T.; Yan, B.; Ma, Y.; Zhang, Z.; Yu, T.; Shen, Z. X.; Chen, H. Y.; Wu, T. *Appl. Phys. Lett.* **2008**, *92*, 173104.
(15) Wang, Z. L.; Song, J. H. *Science* **2006**, *312*, 242.
(16) Wang, X. D.; Song, J. H.; Liu, J.; Wang, Z. L. *Science* **2007**, *316*, 102.
(17) Huang, M. H.; Mao, S.; Feick, H.; Yan, H. Q.; Wu, Y. Y.; Kind, H.; Weber, E.; Russo, R.; Yang, P. D. *Science* **2001**, *292*, 1897.
(18) Sirbuly, D. J.; Law, M.; Yan, H. Q.; Yang, P. D. *J. Phys. Chem. B* **2005**, *109*, 15190.
(19) Pauzauskie, P. J.; Yang, P. *Mater. Today* **2006**, *9*, 36.
(20) Yan, R. X.; Gargas, D.; Yang, P. D. *Nat. Photonics* **2009**, *3*, 569.
(21) Vayssieres, L. *Adv. Mater.* **2003**, *15*, 464.
(22) Greene, L. E.; Law, M.; Goldberger, J.; Kim, F.; Johnson, J. C.; Zhang, Y. F.; Saykally, R. J.; Yang, P. D. *Angew. Chem., Int. Ed.* **2003**, *42*, 3031.
(23) Greene, L. E.; Law, M.; Tan, D. H.; Montano, M.; Goldberger, J.; Somorjai, G.; Yang, P. D. *Nano Lett.* **2005**, *5*, 1231.
(24) Liu, J.; She, J. C.; Deng, S. Z.; Chen, J.; Xu, N. S. *J. Phys. Chem. C* **2008**, *112*, 11685.
(25) Kang, B. S.; Pearton, S. J.; Ren, F. *Appl. Phys. Lett.* **2007**, *90*, 083104.
(26) Li, C.; Hong, G. S.; Wang, P. W.; Yu, D. P.; Qi, L. M. *Chem. Mater.* **2009**, *21*, 891.
(27) Morin, S. A.; Amos, F. F.; Jin, S. *J. Am. Chem. Soc.* **2007**, *129*, 13776.
(28) Hsu, J. W. P.; Tian, Z. R.; Simmons, N. C.; Matzke, C. M.; Voigt, J. A.; Liu, J. *Nano Lett.* **2005**, *5*, 83.
(29) Xu, S.; Wei, Y.; Kirkham, M.; Liu, J.; Mai, W.; Davidovic, D.; Snyder, R. L.; Wang, Z. L. *J. Am. Chem. Soc.* **2008**, *130*, 14958.
(30) Zhou, H. L.; Shao, P. G.; Chua, S. J.; van Kan, J. A.; Bettiol, A. A.; Osipowicz, T.; Ooi, K. F.; Goh, G. K. L.; Watt, F. *Cryst. Growth Des.* **2008**, *8*, 4445.
(31) Cole, J. J.; Wang, X. Y.; Knuesel, R. J.; Jacobs, H. O. *Adv. Mater.* **2008**, *20*, 1474.
(32) Yuan, D. J.; Guo, R.; Wei, Y. G.; Wu, W. Z.; Ding, Y.; Wang, Z. L.; Das, S. M. *Adv. Funct. Mater.* **2010**, *20*, 3484.
(33) Kim, J. H.; Andeen, D.; Lange, F. F. *Adv. Mater.* **2006**, *18*, 2453.
(34) Kelzenberg, M. D.; Boettcher, S. W.; Petykiewicz, J. A.; Turner-Evans, D. B.; Putnam, M. C.; Warren, E. L.; Spurgeon, J. M.; Briggs, R. M.; Lewis, N. S.; Atwater, H. A. *Nat. Mater.* **2010**, *9*, 239.
(35) Kim, J. H.; Kim, E. M.; Andeen, D.; Thomson, D.; DenBaars, S. P.; Lange, F. F. *Adv. Funct. Mater.* **2007**, *17*, 463.
(36) Bengtson, B.; Jagitsch, R. *Ark. Kemi Mineral. Geol.* **1947**, *A 24*, 1.
(37) Peng, H. Y.; Li, G. P.; Ye, J. Y.; Wei, Z. P.; Zhang, Z.; Wang, D. D.; Xing, G. Z.; Wu, T. *Appl. Phys. Lett.* **2010**, *96*, 192113.
(38) Le, H. Q.; Chua, S. J.; Koh, Y. W.; Loh, K. P.; Chen, Z.; Thompson, C. V.; Fitzgerald, E. A. *Appl. Phys. Lett.* **2005**, *87*, 101908.
(39) Andeen, D.; Loeffler, L.; Padture, N.; Lange, F. F. *J. Cryst. Growth* **2003**, *259*, 103.

(40) Pan, H. C.; Chou, C. C.; Tsai, H. L. *Appl. Phys. Lett.* **2003**, *83*, 3156.
(41) Chou, C. C.; Tsai, S. D.; Tu, W. H.; Yeh-Liu, Y. E.; Tsai, H. L. *J. Sol−Gel Sci. Technol.* **2007**, *42*, 315.
(42) Mutaftschiev, B. Nucleation theory. In *Handbook of Crystal Growth*; Hurle, D. T. J., Ed.; North-Holland: Amsterdam, 1994; Vol. 1, Chapter 4.
(43) Andeen, D.; Kim, J. H.; Lange, F. F.; Goh, G. K. L.; Tripathy, S. *Adv. Funct. Mater.* **2006**, *16*, 799.
(44) Boercker, J. E.; Schmidt, J. B.; Aydil, E. S. *Cryst. Growth Des.* **2009**, *9*, 2783.
(45) Yan, X. D.; Li, Z. W.; Chen, R. Q.; Gao, W. *Cryst. Growth Des.* **2008**, *8*, 2406.
(46) Coltrin, M. E.; Hsu, J. W. P.; Scrymgeour, D. A.; Creighton, J. R.; Simmons, N. C.; Matzke, C. M. *J. Cryst. Growth* **2008**, *310*, 584.